Extrinsic fibre Fabry-Perot interferometer for vibration and displacement measurement: the benefit of polarization decomposition

E. Ouisse, Vincent Métivier, Noël Servagent, C. Y. Boisrobert

Extrinsic fibre Fabry-Perot interferometer for vibration and displacement measurement : the benefit of polarization decomposition

Élisabeth Ouisse*[a], Vincent Métivier[a], Noël Servagent[a] and Christian Boisrobert[b]
[a]SUBATECH, UMR École des Mines de Nantes, IN2P3/CNRS, Université de Nantes, 44307 Nantes Cedex 3 - France.
[b]LPIO, Faculté des Sciences de Nantes, BP 92208, 44322 Nantes Cedex 3 - France.

ABSTRACT

We have successfully developed a new design of an extrinsic fibre Fabry-Perot interferometer (EFPI) sensor dedicated to the characterization of vibration and displacement of a target. This device, based on a low finesse Fabry-Perot cavity formed by the end of a 'sensing' optical fibre and the target, gives information on the direction of the motion without the use of an additional reference arm. The incoming light, emitted by a 1310 nm laser diode, is decomposed according to two orthogonal polarization orientation inside the cavity. The two resulting interference signals are then carried back by the same optical fibre and sent to two photodiodes via a coupler and a polarizing beam splitter. With a relatively simple signal processing, a precision of $\lambda/4$ is achieved for the measurement of the displacement, for which the direction is also extracted. In addition, one can determine the velocity of the motion, that have been successfully compared with a reference sensor. The use of a polarization maintaining fibre as sensing arm, not mandatory for monitored laboratory set-up, allows the use of this sensor principle even with external perturbation (temperature changes, mechanical stress,…).

Keywords : optical sensor, optical fibre interferometer, polarization, vibration, displacement measurement.

1. INTRODUCTION

In the past 30 years, extensive study has been done regarding the use of optical fibres as sensors[1,2,3]. Taking advantage of the technical advances carried out by the telecommunication field, combined to their lightweight, small bulk, low sensitivity to corrosion, optical fibres can be used over a wide area of applications. Moreover, they offer the possibility to take away the electronics from the measurement point, allowing no electrical power at this point that can thus be located in relatively extreme environment. Nowadays, optical fibre sensors are present in various domains such as military and space applications, medical, chemical and environmental ones, etc.

There are two kinds of optical fibre sensors: intrinsic and extrinsic ones. For an intrinsic device, the optical fibre is used directly as the measurement object, while for an extrinsic sensor, the optical fibre is only used to guide the information. Both kind of optical fibre sensors (intrinsic and extrinsic) are extensively used as interferometer devices[4,5]. Usual interferometers (Mach-Zehnder, Michelson, Sagnac, etc.) can be designed with optical fibres, avoiding the use of mirrors, which are bulky and fragile, and avoiding major problems of alignment encountered with classical devices. For example, it becomes easy to increase the optical path of a gyros interferometer increasing the length of the optical fibre, increasing thus the sensitivity of the interferometer.

In this paper, we discuss about an extrinsic low-finesse Fabry-Perot interferometer (EFPI) designed for the measurement of target vibration and displacement. Compared to Michelson or Mach-Zehnder interferometers, an EFPI presents the great advantage of not requiring a reference arm. However, the proposed device allows to obtain not only the amplitude of the displacement, like classical EFPI, but also the direction of the motion, using the polarization decomposition of the light to create two sets of signals. In the next two sections, we present the principle of the sensor and the experimental device, including signal processing. In the fourth section, we present the results and performances of the sensor (stability, displacement and velocity measurement, angular tolerance, operating area). Then, some conclusions and perspectives about this work are given.

*Elisabeth.Ouisse@subatech.in2p3.fr ; phone :+(33) 02 51 85 85 60 ; fax :+(33) 02 51 85 84 24

2. PRINCIPLE OF THE EFPI SENSOR :

2.1 Theoretical approach :

A Fabry-Perot interferometer[6,7] is constituted by two parallel and partially reflective interfaces (see Fig. 1.a). An incident light is partially reflected and transmitted by the two interfaces, generating an interference signal pattern, observable either in reflection or in transmission.

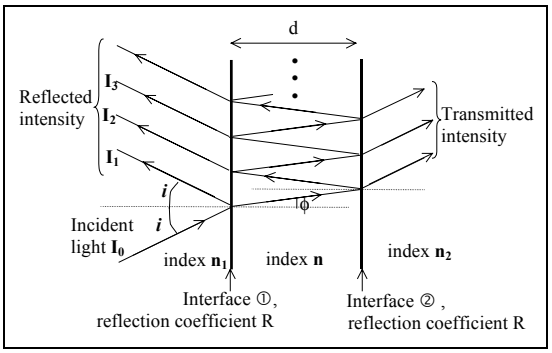

Fig. 1. a) Principle of the Fabry-Perot cavity.

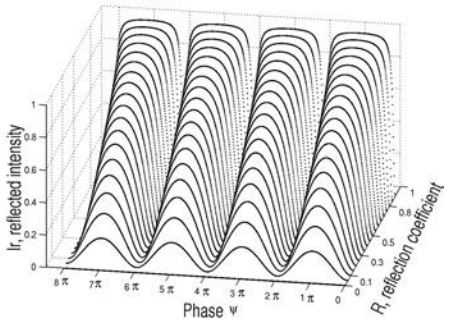

Fig. 1.b) Reflected Intensity for a Fabry-Perot interferometer as a function of its reflection coefficient.

Concerning our EFPI application, only the reflection case has to be considered: interference signals result from the optical path difference between the light reflected by the first interface and transmitted by this interface after one or multiple reflections on the second interface. With I_0 the intensity of the incident beam, one obtains the following formula for the reflected interference signal intensity I_r, where F is the finesse coefficient:

$$I_r = I_0 \frac{F \sin^2\left(\frac{\psi}{2}\right)}{1 + F \sin^2\left(\frac{\psi}{2}\right)} \tag{1}$$

The phase difference ψ is related to the optical path difference δ between the signal reflected by the first and the second interface:

$$\psi = 2\pi \frac{\delta}{\lambda} = 2\pi \frac{n 2d \cos\phi}{\lambda} \tag{2}$$

where the optical path difference $\delta = n\,2d\cos\phi$ is characterized by the index of refraction n inside the Fabry-Perot cavity, its length d and the angle ϕ between the transmitted light and the normal to the interfaces (see Fig. 1.a); λ is the wavelength of the incident light.

The finesse coefficient is written as follows, where R is the reflection coefficient of the interfaces:

$$F = \frac{4R}{(1-R)^2} \tag{3}$$

Thanks to the equation (1), one can plot the intensity (in reflection) of the interference signal I_r versus the phase difference ψ and the reflection coefficient R (see Fig. 1.b). If only a little fraction (less than 10%) of the signal is reflected, the interferometer can be assimilated to a two-beam (or low-finesse) interferometer: the interference signal observed in reflection is quite sinusoidal. In this case, the formula for the resultant intensity I_r for a low-finesse Fabry-Perot interferometer can be express as :

$$I_r = I_1 + I_2 + 2\sqrt{I_1 I_2}\cos\psi \tag{4}$$

where I_1 and I_2 are the intensities resulting from the (first) reflections on the two interfaces and $\psi = \psi_2 - \psi_1$ the corresponding phase difference.

2.2 Extrinsic Fibre Fabry-Perot Interferometer :

In our device, the Fabry-Perot cavity is formed by the cleaved end of an optical fibre and a reflective target (see Figure 2. a)). As only 4% of the incident light is reflected at the fibre-end interface, the device can be assimilated to a two-beam interferometer; the intensity I_r of the resultant interference signal has thus the sinusoidal form described by the equation (4).

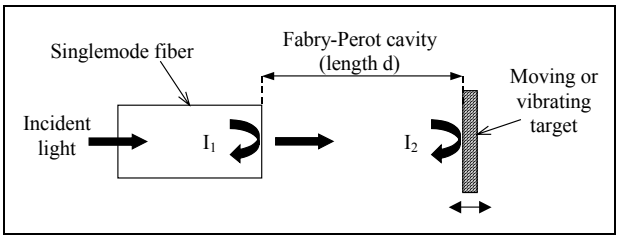

Fig.2. a) Extrinsic Fibre Fabry-Perot interferometer

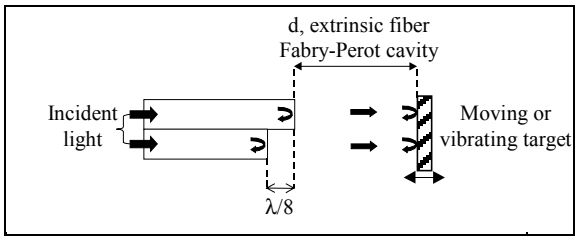

Fig. 2. b) Dual extrinsic Fibre Fabry-Perot interferometer proposed by Claus et al.[8]

Thanks to proper signal analysis, it is possible to measure the displacement or velocity of the moving target. Actually, the displacement of the target corresponds to a change Δd in the length of the cavity, directly related to the phase shift $\Delta\psi$. Considering normal incidence ($\cos\phi = 1$), we obtain from equation (2):

$$|\Delta d| = \frac{\lambda}{n4\pi}|\Delta\psi| \tag{5}$$

According to this formula, we can say that a phase change of 2π is related to a cavity length change of $\lambda/2$ when the index in the cavity is around *1*.

From this, it is also possible to find the velocity of the displacement: $|V_c| = |\Delta d/\Delta t|$.

However, with such sinusoidal interference signal, if it is possible to measure the amplitude and the velocity of the displacement, its direction is not accessible directly. It is so necessary to modify the set-up in order to retrieve this information.

One of the proposed solutions is a quadrature phase-shifted EFPI sensor[8,9]. It consists of a dual interferometer, with two adjacent optical fibres whose fibre-ends are aligned in quadrature (separated from *λ/8*, see Figure 2. b)). The main drawback of such a device is that it is very exigent and constraining at the time of the realization. Moreover it is necessary, during the experiment, to keep the two fibres strictly fixed one to the other.

Another solution is the dual wavelength method10. This approach is characterized by the use of only one Fabry-Perot cavity but two sources of close wavelengths λ1 and λ2. Thanks to these two sources, the two interference signals are slightly different and the direction of the motion can be determined .

2.3 Our sensor principle :

In order to overcome these difficulties, we have realized a single fibre EFPI[11]. Using polarization properties of light, two sets of interference signals can be propagated in the same fibre at the same time. Actually, the light can be described in terms of the electric field **E**(*z*,*t*) of an electromagnetic wave, where *z* is the direction of propagation and *t* the time. This field can be separated in two orthogonal components $\mathbf{E}_x$ and $\mathbf{E}_y$, each perpendicular to the direction of propagation :

$$\mathrm{E}(z,t) = \underbrace{E_{x0}\cos(\omega t - kz)\boldsymbol{x}}_{\mathrm{E_x}} + \underbrace{E_{y0}\cos(\omega t - kz + \Delta\theta)\boldsymbol{y}}_{\mathrm{E_y}} \tag{6}$$

where E_{x0} (resp. E_{y0}) is the amplitude of the field $\mathbf{E}_x$ (resp. $\mathbf{E}_y$); ω is the pulsation and $\Delta\theta$ the phase difference between $\mathbf{E}_x$ and $\mathbf{E}_y$.

If we are able to separate this two components, we can obtain two separated interference signals related to the components $\mathbf{E}_x$ and $\mathbf{E}_y$ that can be propagated in the same fibre.

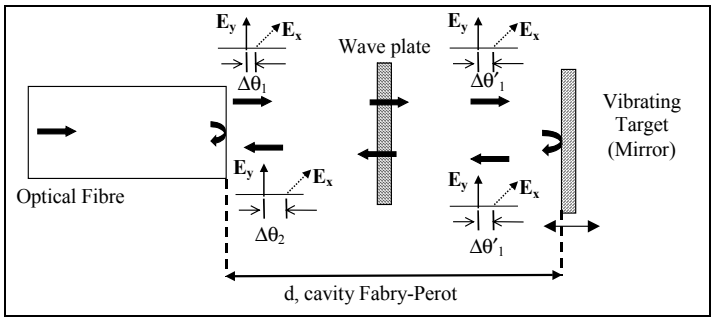

Fig. 3. One interferometer with two interference signals and only one measurement arm.

By introducing a wave plate in the Fabry-Perot cavity (see Figure 3), we delay one of two orthogonally polarized components of incident light. As shown in Figure 4, with this device the interference signals may be in quadrature and it is possible to determine without ambiguity the direction of target motion. When the direction of the target changes, the advance or delay of one interference signal compared to the other changes ($\Delta\tau$ is > 0 or < 0).

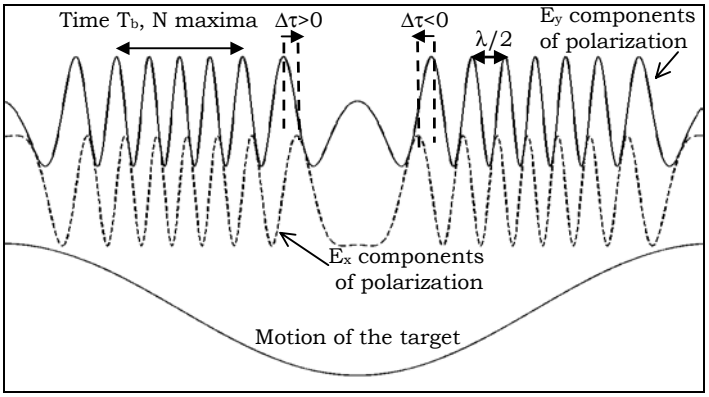

Fig.4. The two separated (E_x and E_y components) interference signals simulated as a function of the target motion.

We have already noted that between two maxima in the interference signal the target has moved of $\lambda/2$; by simply counting these peaks and without interpolation, we obtain a precision of half a wavelength on the displacement.

Moreover, with such interference signals, by considering a linear portion, we can calculate the beat frequency f_b. This last is a function of the number N of maxima during the time T_b and may be estimated by :

$$f_b = \frac{N-1}{T_b} \tag{7}$$

The phase change $\Delta\psi$ for a beat frequency f_b is given by :

$$\Delta\psi = 2\pi\,\Delta t\, f_b \tag{8}$$

where Δt is the time corresponding to the phase shift $\Delta\psi$. From equation (5), one can determine the change of cavity length, and then the velocity of the vibrating target $V_c = \Delta d/\Delta t$ as a function of the beat frequency f_b :

$$V_c = \lambda/2.f_b \tag{9}$$

Sensors based on the principle described above would offer very appealing advantages. Such devices allow us very easily to know the velocity and the displacement of a vibrating target. Moreover the introduction of a wave plate in the cavity and the use of the polarization properties of light allows to deal with the determination of the direction of the motion. In the next section, we will describe the corresponding experimental device.

3. EXPERIMENTAL DEVICE

We have designed an experimental device based on the physical principle described previously. It is constituted of three major parts (see Figure 5) connected thanks to an optical fibre coupler :

- a light source (a pigtailed DFB laser diode module operating at *1310 nm* with an optical power around *2 mW*).

- a sensing arm (including the sensor head) based on a polarization maintaining fibre (Panda^{TM} type). A mirror fixed on the piezoelectric transducer (PZT) serves as vibrating target.

- an analysis arm, which permits the observation of the interference signals via two photodiodes. A polarizing beam splitter is used to separate the two components E_x and E_y.

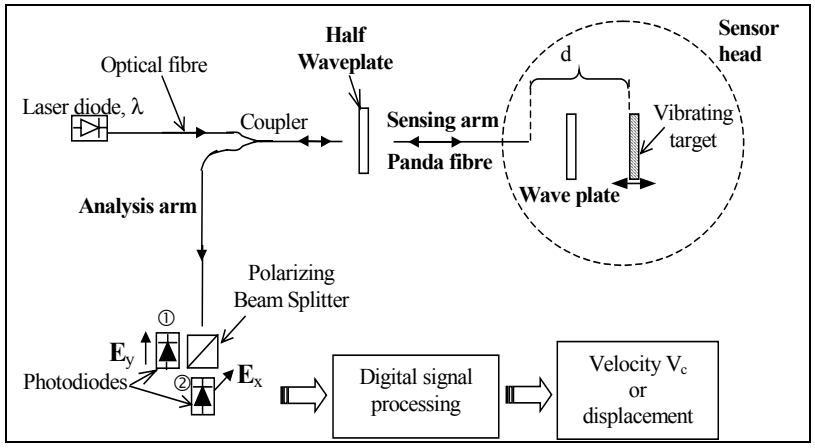

Fig. 5. Schematic view of the extrinsic optical fibre Fabry-Perot interferometer.

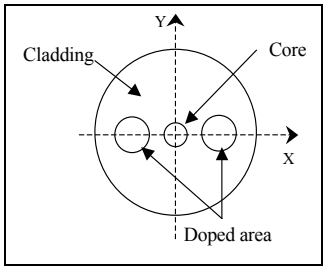

Fig. 6. Cross section of the Panda^{TM} fibre

The use of optical fibres allows to locate the electronic devices (laser diode, photodiodes) far away from the measurement point. However, instability of the polarization can appear when the optical fibre is stressed. This is why the sensing arm requires a particular attention. To prevent this problem, we have replaced classical fibre by a Panda^{TM} type polarization maintaining fibre. This fibre is constituted by a circular core and an optical cladding, with stressed regions (highly doped) around the core (see Figure 6). The incident polarization is injected with an angle of 45° between the two main axes (named here X and Y) to maintain the components E_x and E_y of the polarization. Consequently, we insert at the input of this fibre a half wave plate used to adjust the angle of incident polarization.

In a first step, the data are acquired on a computer via an oscilloscope. The oscilloscope is triggered to observe only a linear portion of the target motion. Thus the beat frequency of the interference signal is almost constant. With such configuration, we can measure the stability of the device, the angular tolerance and compare the sensor with another one (see 4.1, 4.3 and 4.2.).

In a further step, this data processing, convenient for laboratory measurement, is replaced by digital signal processing (DSP) for real time measurement (see Figure 7.).

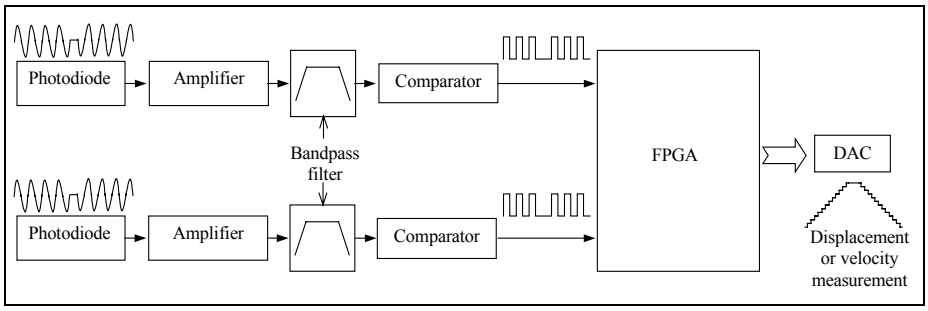

Fig.7. Simplified block diagram of the signal processing.

The Figure 7. illustrates the different steps of the digital signal processing. The interference signals collected by the photodiodes are amplified and passed through a band pass filter that eliminates the DC component and the high frequencies of the signal.

A comparator then detects the zero-crossing of both analog interference signals. The output binary signal is set to 1 for positive input signal. Pulses are generated in the Field Programmable Gate Array (FPGA) for each up and down edges: two successive pulses correspond to a displacement of the target of $\lambda/4$. A counter is then incremented or decremented as a function of the direction of the motion. Moreover, when the interference signals are strictly in quadrature, one can use both in the same analysis and displacements of $\lambda/8$ are reachable.

4. RESULTS AND PERFORMANCES

4.1 Stability :

In order to ensure the frequency stability of the device, we have measured the interference signal beat frequency during several hours, without changing the speed control of the PZT. To complete this experiment, the room temperature is also measured. The Figure 8 displays the obtained results.

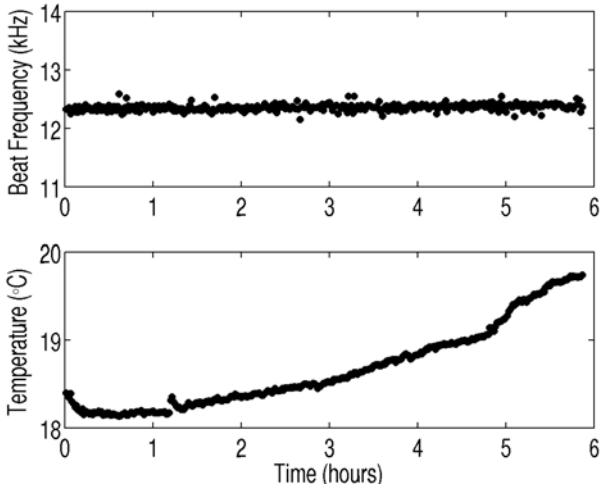

Fig. 8. The beat frequency stability and the room temperature changes over six hours.

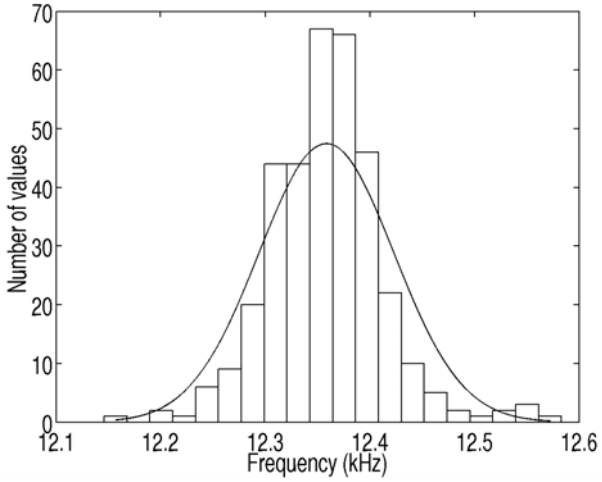

Fig. 9. Statistical distribution of the frequency measurement and gaussian fit.

The Figure 8 establishes that the frequency measurement is independent of the room temperature changes. It turns out that for this experiment the beat frequency ($\overline{f_b}$) is 12360 *Hz* with a standard deviation (σ) of 125 *Hz*. Considering a width of $\pm 2\sigma$ (covering 95% of the values), we note that we obtain a reduced spread in the measurements (250 *Hz* represent a dispersion of about 2 %). We have so demonstrated the good stability of the experiment.

4.2 Comparison with a reference sensor :

Previous operations has proved the stability of beat frequency measurement with an accuracy of 2%. We now compare our measurements with those of a reference sensor[12], based on the self-mixing phenomenon. The two devices are placed parallel one to the other and perpendicular to the target. The results obtained with the two sensors are found to be in good agreement (see Figure 10). Each experimental point represents the average of ten measurements at a given beat frequency and the error bar stands for the maximum dispersion.

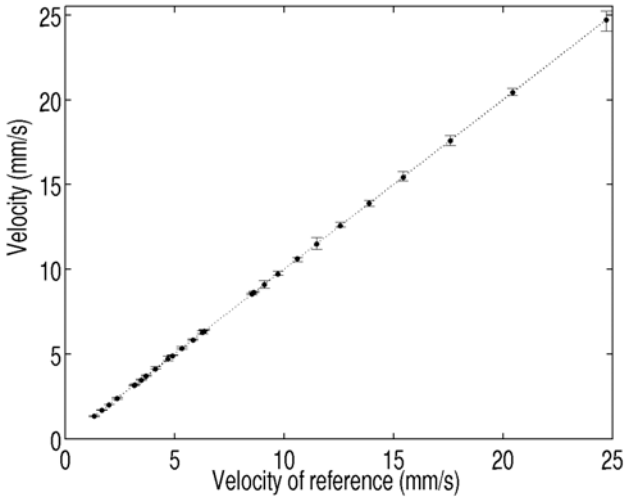

Fig. 10. Comparison of the velocity measurement between a reference device and our sensor with a PZT excitation amplitude of 1,3 V_{pp} while a variable frequency.

4.3 Displacement reconstruction :

Two experimental interference signals (related to the two orthogonal components of the polarization) are represented in the bottom part of the oscilloscope screen captures shown in Figure 11. One can note they are effectively in quadrature and that the corresponding phase shift depends on the direction of the motion (left and right part). The upper part of these figures represent the reconstructed displacement obtained thanks to the signal processing performed by the DSP (see part 3 and Figure 7). We obtain a displacement reconstruction by steps of $\lambda/8$ for both directions.

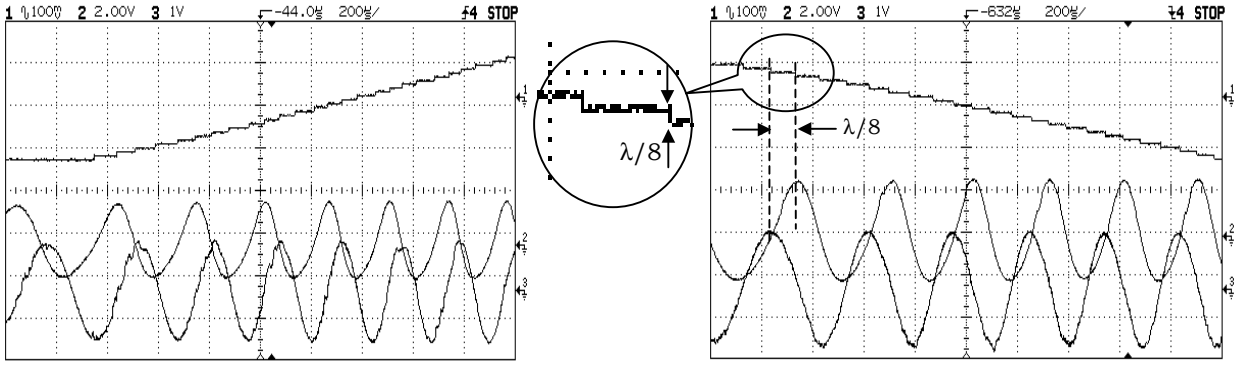

Fig. 11. Experimental reconstruction's of the target motion by data processing.

These interference signals are obtained with a mirror fixed on a moving target; in this configuration, we must take care of the alignment between the sensing fibre and the target. An introduction of a tilt of less than one degree is enough to disturb the interference signals. However, we have observed (see Figure 12) a very interesting feature when the mirror target and the fibre-end are slightly misaligned: the beat frequency is doubled. This phenomenon has already been reported in the literature[13] and is due to a quadruple stroke in the cavity. This configuration allows to double the sensitivity of the device for the displacement measurement.

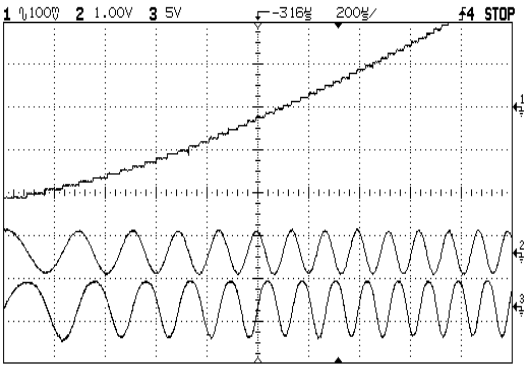

Fig. 12. Experimental reconstruction of the target motion by signal processing with steps of $\lambda/16$.

When the angle between the fibre-end and the target increases, the amplitude of interference signals decreases drastically. The angular tolerance between the fibre-end and the target is relatively short (around 2-3 degree). Beyond of this limit, the light reflected on the mirror is not reinjected and we don't observe any more interference signals.

In order to increase this limit angle, we have identified retro-reflective targets that reflect the signal in the same direction as the incident signal.

4.4 Angular tolerance for retro-reflective target :

Among the retro-reflective target, we choose to use the micro prisms or micro spheres because they have the great advantage of being very compact and simple to fix on the target. We choose the micro prims because our samples are also distributed and their size are more regular than those of micro spheres. The Figure 13 is the photograph of our micro prisms sample, we have estimated that the size of the micro-prisms have a pitch of around *500 µm*.

Fig. 13. Photographs of the micro prisms retro reflective target

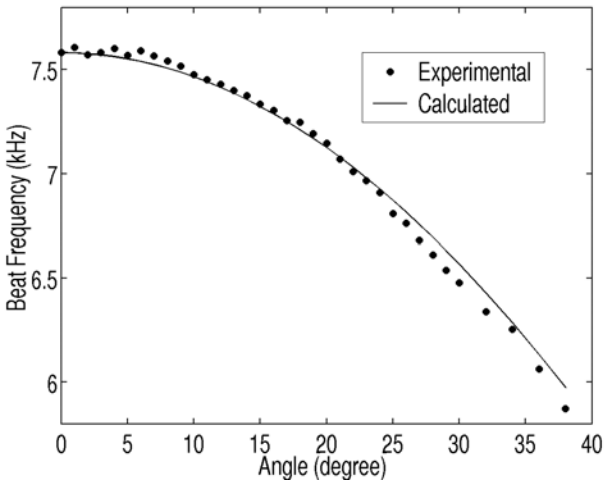

Fig. 14. Measurement of vibration frequency as a function of the incidence angle between the fibre-end and the target (micro prisms).

Experiments were performed by replacing the mirror by a sample of micro-prisms on the PZT. They consist of measuring the frequency with the EFPI sensor and to find the limit angle beyond which the signal vanishes.

As shown in Figure 14, the frequency measured with our interferometer is function of the angle between the fibre-end and the preparing target. With the micro-prism, the maximum angle from which it is possible to measure the frequency is around 35°. Beyond, the signal is not reflected in the same direction as the incident signal and so, we will not have any more interference signal. The calculated curve is obtained by multiplying the experimental frequency measured at the angle zero by the cosine of the theoretical angle between the fibre-end and the vibrating target. This calculated curve serves as a guideline and to validate the experimental results.

But these targets seems to be birefringent, since they change the polarization of light after reflection. So their use is not compatible with our principle of determination of the direction of the motion. That is the reason why we currently use mirror as target, although the angular limit with this latter is smaller (around 2-3°).

4.5 Operating area :

The operating area of the sensor is determined by identifying limits (amplitude and frequency of vibrations of the target) beyond which the response of the EFPI sensor is no longer available (see Figure 15.). It depends on some parameters, like elementary displacement step, DAC range, etc.

Concerning next example, we have considered that the displacement of the target is rebuilt by step of λ/2. This choice allows us a good balance between the precision measurement and the range (in amplitude and frequency) achievable.

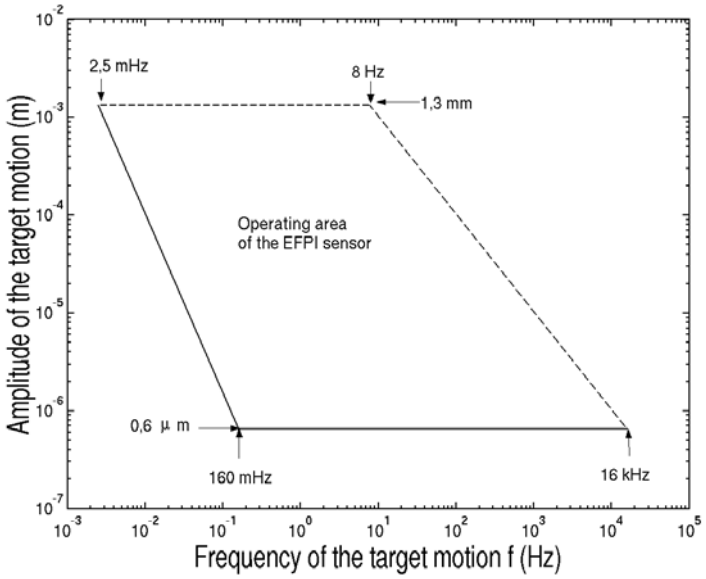

Fig. 15. Operating area of our Extrinsic Fibre Fabry-Perot Interferometer (EFPI)

By considering a linear portion of the displacement, we can express the velocity as :

$$V = 2\pi.A.f \tag{10}$$

where A and f are respectively the vibration amplitude and the beat frequency of the target.

With regard to the amplitudes, the minimum ($A_{\min}$) is given by the optical limit in such a way that :

$$A_{\min} = \frac{\lambda}{2} \approx 0{,}6\mu m \tag{11}$$

The maximum amplitude ($A_{\max}$) is driven by the characteristic of the digital to analog converter (DAC). With a 12 bits DAC, we have 4096 possible values between $-A_{\max}$ and $+A_{\max}$:

$$A_{\max} = 2048.\frac{\lambda}{2} \approx 1{,}3mm \tag{12}$$

In our present configuration, photodiode electronics limits the band pass of the frequency between *1 Hz* and *100 kHz*. The corresponding velocities are calculated by inserting these limits in the equation (9) :

$$V_{c\max} \approx 6{,}55\,cm/s \tag{13}$$

$$V_{c\min} \approx 0{,}655\,\mu m/s \tag{14}$$

By introducing the numerical values of $A_{\min}$, $A_{\max}$, $V_{c\ \min}$ and $V_{c\ \max}$ into equation (10), the minima (2,5 and 160 mHz) and maxima (8 *Hz* and 16 *kHz*) of the frequencies are calculated (see Figure 15.).

These limits are only due to the electronics employed and should be easily enlarged: in order to increase the maximum amplitude (A_{max}) achievable, one have only to use a DAC with larger dynamics; by optimizing the photodiode electronics, one will increase the value of the maximum frequency f_{max}.

5. CONCLUSIONS

We have demonstrated the principle of a new extrinsic fibre Fabry-Perot interferometer for the direct measurement of vibration amplitude and frequency of a vibrating target with a precision of $\lambda/4$ on displacement measurement. By using the polarization properties of the light and inserting a wave plate into the external cavity, we are able to determine the direction of the motion target. Thus we have developed a versatile device, with the great advantage of using only one source (λ=1310 nm), one sensing fibre and one cavity to determine the velocity or the displacement of a moving target.

It has been also demonstrated that the use of a polarization maintaining fibre for the sensing arm provides unambiguously the direction of the motion and will make the use of the sensor out of the laboratory more convenient.

We have also presented succinctly the digital signal processing and the operating area of the sensor has been demonstrated. By improving the electronics of the photodiodes and the digital signal processing, the present limits of our sensor will be improved.

REFERENCES

1. D. A. Jackson, *Monomode optical fibre interferometers for precision measurement*, J. Phys. E: Sci. Instrum., Vol. 18, pp. 981-1001, 1985.

2. B. E. Jones, *Optical fibre sensors and systems for industry*, J. Phys. E: Sci. Instrum., Invited keynote paper, Vol. 18, pp. 770-782, 1985.

3. A. D. Kersey, *A Review of Recent Developments in Fibre Optic Sensor Technology*, Optical Fibre Technology, Vol. 2, pp. 291-317, 1996.

4. E. Udd, *An overview of fibre-optic sensors*, Rev. Sci. instrum., Vol. 66, 1995, pp. 4015-4030.

5. B. Culshaw, *Optical systems and sensors for measurementand control* , J. Phys. E: Sci. Instrum., Invited review article, Vol. 16, 1983, pp. 978-986.

6. J. M. Vaughan, *The Fabry-Perot Interferometer History, Theory, Practice and Applications*, Adam Hilger Series on Optics and Optoelectronics, 1989, Chap. 3, pp. 89-134.

7. T. Yoshino, K. Kurosawa, K. Itoh and T. Ose, *Fibre-Optic Fabry-Perot Interferometer and Its sensor Applications*, IEEE Journal of Quantum Electronics, Vol. QE-18(10), 1982, pp. 1624-1633.

8. R. O. Claus, M. F. Gunther, A. Wang and K.A. Murphy, *Extrinsic Fabry-Perot sensor for strain and crack opening displacement measurements from –200 to 900°C*, Smart Mater. Struct., Vol. 1, 1992, pp. 237-242.

9. V. Bhatia, K.A. Murphy, R. O. Claus, M. E. Jones, J. L. Grace, T. A. Tran and J. A. Greene, *Multiple strain state measurements using conventional and absolute optical fibre-based extrinsic Fabry-Perot interferometric strain sensors*, Smart Mater. Struct., Vol. 4, 1995, pp. 240-245.

10. O. B. Wright, *Stabilized dual-wavelength fiber-optic interferometer for vibration measurement*, Opt. Lett., Vol. 16, 1991, pp. 56-58.

11. H. C. Seat, E. Ouisse, E. Morteau, V. Metivier, *Vibration-displacement measurements based on a polarimetric extrinsic fibre Fabry-Perot interferometer*, Meas. Sci. Technol., Vol. 14, 2003, pp. 710-716.

12. F. Gouaux, N. Servagent and T. Bosch, *Absolute distance measurement with an optical feedback interferometer*, Appl. Opt., Vol. 37, 1998.

13. R. Addy, A. W. Palmer and K. T. V. Grattan, *Effects of External Reflector Alignment in Sensing Application of Optical feedback in Laser Diodes*, Journal of Lightwave Technologie, Vol. 14(12), 1996, pp. 2672-2676.